Progress In Electromagnetics Research, Vol. 155, 105–113, 2016

Ultra-Compact Multi-Band Chiral Metamaterial Circular Polarizer Based on Triple Twisted Split-Ring Resonator

Yongzhi Cheng[1, 2, *], Chenjun Wu[2], Zhengze Cheng[3], and Rongzhou Gong[2]

Abstract—An ultra-compact chiral metamaterial (CMM) using triple-layer twisted split-ring resonators (TSRRs) structure was proposed, which can function as a multi-band circular polarizer. This ultra-compact structure CMM can convert an incident linearly y-polarized (x-polarized) wave propagating along the $-z(+z)$ direction to the transmitted left circularly polarized (LCP) waves at 7.28 GHz, 13.22 GHz and 15.49 GHz while the right circularly polarized (RCP) waves are at 9.48 GHz simultaneously. In addition, the large polarization extinction ratio (PER) of more than 20 dB across four resonance frequencies can be achieved. The experiment results are in good agreement with the numerical simulation results. The surface current distributions of the structure are analyzed to illustrate this linear to circular polarization conversion. The unit cell structure is extremely small both in longitudinal and transverse directions. Good performances and compact design of this CMM suggest promising applications in circular polarizers that need to be integrated with other compact devices.

1. INTRODUCTION

Chiral metamaterials (CMMs) is lack of any mirror symmetry and also neither violates reciprocity nor time-reversal symmetry, which has been paid attention increasingly due to their exotic electromagnetic (EM) properties [1–9]. From microwave to optical ranges, negative refraction [1], giant gyrotropy [2], optical activity [3–6], circular dichroism (CD) [7–9], asymmetric transmission (AT) [10–13], and linear or/to circular polarization conversion [14–16] can be explored and realized by special CMM design. Essentially, these unique EM properties mainly originate from cross-coupling of the electric and magnetic fields among these chiral structures [17–23]. In effect, the coupling mechanisms have been studied in detail at microwave and optical frequencies. Optical activity and CD effect have also been observed [24, 25]. On these peculiarities, the giant CD effect for circular polarization is very important, which has many potential applications, such as antennas [26], liquid crystal displays and remote sensors [27, 28]. It is highly desirable to design high-performance circular polarizer or circular polarization convertor. CMMs based circular polarizer has some advantages in a compact design scheme and scaled to different EM spectrum due to the geometry scalability. For the CMMs based circular polarizer, firstly, Gansel et al. proposed a broadband circular polarizer based on three-dimensional (3D) gold helices at infrared region [29]. However, only one kind of circularly polarized waves could be obtained by such a helix CMM, which is hard to fabricate and integrate into present microwave systems. Later, a photonic CMM composed of twisted split-ring-resonator was proposed, where a significant circular polarized wave with different rotation directions at two distinct resonances was observed [20]. Then, four U-shaped split ring structures with different sizes [30], planar bi-layer spiral

Received 25 January 2016, Accepted 23 February 2016, Scheduled 14 March 2016

* Corresponding author: Yongzhi Cheng (chengyz@wust.edu.cn).

[1] Engineering Research Center for Metallurgical Automation and Detecting Technology, Ministry of Education, Wuhan University of Science and Technology, 430081, P. R. China. [2] School of Optical and Electronic Information, Huazhong University of Science and Technology, Wuhan, Hubei 430074, P. R. China. [3] School of Electronic and Information Engineering, Hubei University of Science and Technology, Xianning 437100, P. R. China.

structures [31, 32], twisted split ring resonators (SRRs) with double rings [33], Hilbert-shaped structure and other novel asymmetric CMMs [34–38] have afterwards been intensively reported. Among them, nearly all these CMMs could be available to tailor the cross coupling between electric and magnetic fields, resulting in a giant CD effect for circular polarization at resonances [39]. However, multi-band or bandwidth expansion is still a main concern which needs improvement. An effective method is stacking metallic-dielectric multilayer planar structure [40], which gives some new ideas for multi-band or broadband device design for polarization transformation [11, 25, 40, 41].

In this work, an ultra-compact CMM using multilayer-stacked system is proposed, which is capable of emitting circularly polarized waves from incident linearly polarized wave at four resonances under normal incidence. A strategy of stacking metal-dielectric multilayer planar structure is shown to dramatically excite the multi-resonance modes. From the bottom to the top, there are three layers of SRRs with double ring structures stacked with the angle of mutual twist $\alpha = 45°$. The simulated and measured results demonstrate that when a plane wave with $y(x)$ direction linear polarization is incident on this CMM slab propagating along $-(+)z$ direction, circular polarization waves with different rotation directions and high polarization extinction ratio (PER) are obtained at four distinct resonances. In addition, the unit cell of the structure is extremely small in all three dimensions simultaneously compared with the operation wavelengths, which can be integrated easily with other electrical small devices such as antennas or sensors in lower frequency.

2. FUNDAMENTAL THEORY, AND UNIT-CELL STRUCTURE DESIGN

Firstly, we briefly recall some fundamental theories of the CMMs for circular polarizer or circular polarization convertor before characterizing the polarization characteristics of our design. Under the Cartesian coordinates of x-y-z, considering an incident EM wave propagating in the $+z$ direction, the expressions of electric field vector of incident and transmitted wave along x-polarized and y-polarized direction are as following [17]:

$$\mathbf{E}^i(r,t) = \begin{pmatrix} E_x^i \\ E_y^i \end{pmatrix} e^{i(kz-\omega t)} \tag{1a}$$

$$\mathbf{E}^t(r,t) = \begin{pmatrix} E_x^t \\ E_y^t \end{pmatrix} e^{i(kz-\omega t)} \tag{1b}$$

where ω, k, E_x, and E_y represent the angular frequency, wave vector, and complex amplitudes of EM wave, respectively. The transmission coefficient $t_{ij} = E_i^t/E_j^i$ is defined in terms of complex amplitude of the electric field, with the first and second subscripts i and j ($= x, y$ for linear polarization, $= +, -$ for circular polarization) denoting the polarized states of the transmitted wave and incident wave components, respectively. It is indicated that an arbitrary plane linear polarization wave through certain CMMs slab can be decomposed into different components (E_x^t and E_y^t) of the transmitted EM waves through the above transmission coefficients (the complex Jones matrix). For our designed CMMs, the transmitted circularly polarized waves with two orthogonal polarization eigenstates right-handed circularly polarized (RCP, $+$) and left-handed circularly polarized (LCP, $-$) waves associated with the two incident orthogonal linearly polarized components can be expressed as [22, 31]:

$$t_{cir\text{-}lin} = \begin{pmatrix} t_{+x} & t_{+y} \\ t_{-x} & t_{-y} \end{pmatrix} = \begin{pmatrix} t_{xx} + it_{yx} & t_{xy} + it_{yy} \\ t_{xx} - it_{yx} & t_{xy} - it_{yy} \end{pmatrix} \tag{2}$$

where t_{+x}, t_{-x}, t_{+y} and t_{-y} are the four RCP and LCP transmission coefficients from the linear to circular polarization conversion, which indicates the capability of the CMM to convert an EM wave with linear to circular polarization [30–34]. Moreover, the substantially large or small difference (PER) between the RCP and LCP waves can be calculated as:

$$\mathrm{PER} = 20\log_{10}\left(|t_{+x(y)}|/|t_{-x(y)}|\right) \tag{3}$$

Thus, we can also use the PER to characterize the circular polarization conversion efficiency of the transmitted waves. The transmission coefficients and PER should be as high as possible for the circular polarizer or circular polarization convertor in engineering. Generally, the polarization properties of the

transmitted EM waves can be characterized by the polarization rotation angle θ and ellipticity angel η. The polarization rotation angle θ represents the rotation angle between the polarization planes of the transmitted and incident waves when linearly polarized wave passes through a CMM slab. Thus, we can use θ to characterize the rotation property of the transmitted waves. On the other hand, η characterizes polarization state of the transmitted wave and also measures the CD effect due to the difference of RCP and LCP waves in magnitudes. Polarization azimuth rotation angle θ and ellipticity angle η for the normal incident wave can be expressed by the following formulas [17, 41]:

$$\theta = \frac{1}{2}\tan^{-1}\left(\frac{2p\cos(\varphi)}{1-p^2}\right) \tag{4}$$

$$\eta = \frac{1}{2}\sin^{-1}\left(\frac{2p\sin(\varphi)}{1+p^2}\right) \tag{5}$$

where $p = |t_{xy}/t_{yy}|$ and $\varphi = \arg(t_{xy}) - \arg(t_{yy})$. Note that the transmitted wave will be purely circular and linear polarization if η equals $\pm 45^\circ$ and 0°, respectively. Otherwise, the transmitted wave is elliptically polarized if η is between 0° and 45°, -45° and 0°.

To go a step further, we will demonstrate our proposed CMMs numerically and experimentally for the multi-band circular polarization conversion. Since the split-ring resonators (SRRs) allow for a control and manipulation of EM (light) waves on sub-wavelength length scales [8, 12, 14, 15, 23], which is also employed as the basic element in our design. Figs. 1(a), (b) show the unit cell structure of the designed CMM in detail. As shown in Fig. 1(a), the designed CMM is composed of three metallic layers and two dielectric spacer layers from the top to bottom layers. Similarly to the unit cell structure configuration in [11, 41], the split direction of DSRRs is rotated in a certain angle α along axial direction. The DSRRs in the two layers are coaxial but mutually twisted by $\alpha = 45^\circ$. The front DSRR pattern is formed by rotating an enantiometric form of the back DSRR by 90°. This construction law in our design distinguishes any previous design with only a mutual 90° twist or with only an enantiometric form [3–9]. Thus, the chirality of the design can be further enhanced. The DSRRs have undergone several miniaturized refinements in an attempt to optimize the resonances supported in the structure as four resonances hold the key in tailoring the cross-coupling of chiral structures between the electric and magnetic fields. Thus, circular dichroism and optical activity can be expected. The EM response of the normally incident wave with x polarization is different from that with y polarization since no line of mirror symmetry and any four-fold rotational symmetry (C_4) can be observed. In our design, circular polarization waves can only be obtained in the case of incident $y(x)$-polarized wave propagating along $-z(+z)$ direction. We demonstrate our proposed CMMs for multi-band circular polarization conversion through numerical simulation and experiments. The dielectric substrate is chosen to be an FR-4 board with relative permittivity of 4.2 and dielectric loss tangent of 0.025. The metallic structure layers in both sides are modeled as a 0.02 mm copper film with an electric conductivity $\sigma = 5.8 \times 10^7$ S/m. The optimized geometry parameters are as follows: $p = 3.5$ mm, $t_s = 0.55$ mm, $r_1 = 1.1$ mm, $r_2 = 1.6$ mm, $w = 0.25$ mm, $g = 0.4$ mm.

3. SIMULATION AND EXPERIMENT

To study the polarization conversion characteristic of the designed CMMs, the numerical simulations are performed using the standard finite difference time domain (FDTD) method. In the simulation, the unit cell boundary condition is applied to the transverse boundaries to replicate an infinite planar array, while perfectly matched layers are applied to the z direction. The designed CMMs are fabricated by the conventional printed circuit board (PCB) process, and a photograph of the fabricated sample is depicted in Fig. 1(d). The total area of the fabricated sample is 196×196 mm^2, containing 56×56 unit cells. Agilent PNA-X N5244A vector network analyzer connected to the two standard gain broadband linearly polarized horn antennae is employed to measure the fabricated CMM sample in an EM anechoic chamber. The CMM slab is placed in the middle of the horn antennas. Both antennas own VSWR < 2 and face each other with a distance of 1 m over a wide frequency range of 5 to 17 GHz to eliminate near-field effect [30]. When a broadband plane EM wave with y-polarization is normally impinged on the designed CMM slab propagating along $-z$ direction, the transmission coefficients of co-polarization t_{yy} and cross-polarization t_{xy} are obtained. The plane waves with different linear polarizations are

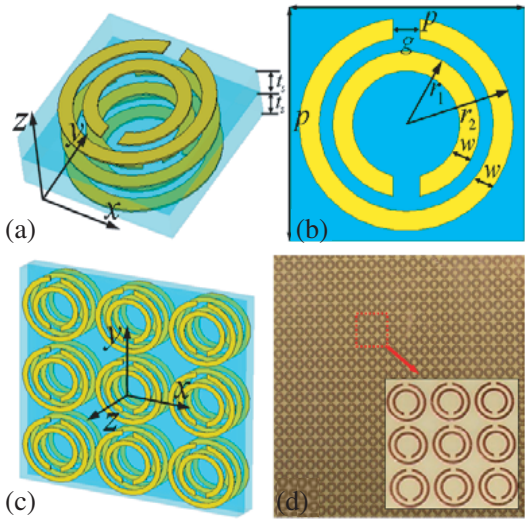

Figure 1. (a), (b) The perspective view and front view of the unit cell structure of the designed CMMs, (c) three dimensional array structure, (d) photograph of the fabricated sample.

generated and received by rotating the orientation of the two horn antennas. For both simulation and experiment, according to above Eq. (2), the transmitted circular polarization coefficients can be expressed as $t_{\pm} = t_{xy} \pm it_{yy}$, where the subscripts "+" and "−" denote the RCP and LCP waves, respectively. As a circular polarizer or circular polarization convertor, the difference between the RCP wave and LCP wave transmission coefficients for linear to circular polarization conversion and the efficiency should be as high as possible in engineering. The electric response for the normally incident x-polarized wave distinguishes from that for the y-polarized wave due to the lacking of C_4 symmetry of the proposed structure [34]. Thus, for our design, the giant circular dichroism and good performances of the circular polarization can be valid only for the y-polarized waves propagating along $-z$ direction.

4. RESULTS AND DISCUSSIONS

Figure 2(a) presents the simulated and measured co- and cross-polarization transmission coefficients for the normal incident y-polarized wave propagating along $-z$ direction. A good agreement of results between simulation and experiment is observed across the whole frequency range. As shown in Fig. 2(a), four resonant frequencies are observed at $f_1 = 7.15\,(7.28)$ GHz, $f_2 = 9.24\,(9.38)$ GHz, $f_3 = 13.22\,(13.29)$ GHz, and $f_4 = 15.34\,(15.45)$ GHz from the co- and cross-polarization transmission coefficients (t_{yy} and t_{xy}) in experiment (simulation). There are slight frequency shifts between

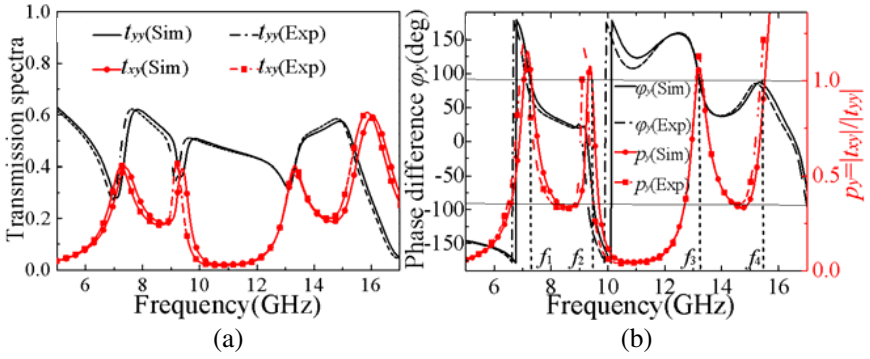

Figure 2. Simulated and measured results for the designed CMM: (a) the co- and cross-polarization transmission coefficients (t_{yy} and t_{xy}), (b) the ratio p_y and phase difference φ_y between the co- and cross-polarization.

simulation and measurement curves due to the tolerances occurring in the fabrication and measurements. Simulation and measurement results indicate that the peak amplitudes of t_{yy} and t_{xy} are nearly the same and are about 0.5 around above four resonance frequencies. In order to demonstrate the linear-to-circular polarization conversion, the ratio of transmission coefficients $p_y = |t_{xy}|/|t_{yy}|$ and phase difference $\varphi_y = \arg(t_{xy}) - \arg(t_{yy})$ for cross-polarization and co-polarization are also calculated. The corresponding results are depicted in Fig. 2(b). The simulated values of ratio p_y are about 1.05, 1.01, 1.12 and 0.98, while the phase differences φ_y are 90.6°, −91.2°, 89.5° and 88.7° at 7.15 GHz, 9.44 GHz, 13.19 GHz and 15.34 GHz, respectively, which are in good agreement with measurements. Thus, the high conversion efficiency for linear-to-circular polarization can be unambiguously demonstrated. These results suggest that nearly pure circular polarization waves with different rotation directions can be obtained around four resonances after the y-polarized wave passing through the designed CMMs slab propagating along forward $(-z)$ direction.

Taking a further step, the simulated and measured normalized linear-to-circular polarization transmission coefficients are depicted in Fig. 3(a). It can be observed that there are significant differences between the RCP and LCP waves in the frequency band ranging from 5 GHz to 17 GHz. The measured (simulated) transmission coefficients for the LCP wave reach their minimum values about 0.037 (0.021), 0.056 (0.021) and 0.062 (0.055) at 7.15 (7.28) GHz, 13.19 (13.22) GHz, and 15.34 (15.45) GHz, respectively. However, the transmission magnitudes for the RCP wave are 0.77 (0.749), 0.788 (0.777) and 0.844 (0.839). To further demonstrate the differences between the transmissions of the RCP and LCP waves and circular polarization conversion efficiency for our designed CMM, we also calculate the PER according to Eq. (3), and the corresponding results are depicted in Fig. 3(b). From Table 1, it can be observed that the measured (simulated) PERs are about 26.11 (30.84) dB, 20.95 (30.46) dB and 23.15 (23.76) dB at the above three frequencies, which further indicate that the transmitted EM waves are the relatively pure RCP. At another resonance frequency of 9.24 (9.38) GHz, the transmission coefficient for LCP waves is 0.78 (0.765), while one of the RCP waves is as low as 0.045 (0.057). The PER is 22.61 (26.22) dB as shown in Fig. 3(b), indicating that the LCP wave is obtained from a y-polarized incident wave after it travels through the designed CMM at this resonance. It is revealed that the incident y-polarized (x-polarized) waves along the $-z$ ($+z$) directions can be converted well to nearly pure RCP and LCP waves around the four resonances after passing through

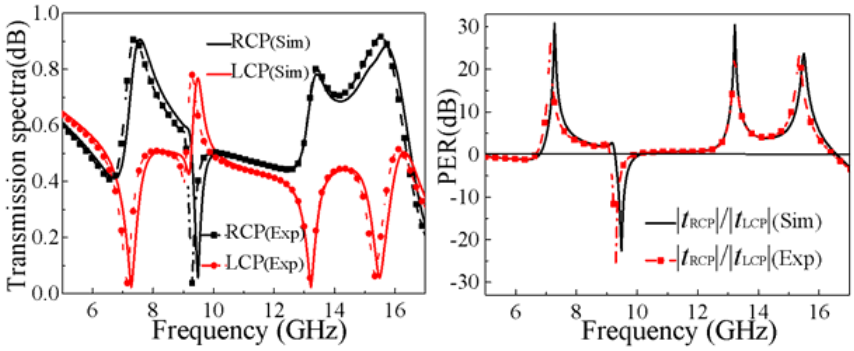

Figure 3. Simulated and measured (a) transmission spectra of the LCP and RCP waves for linear to circular polarization conversion, (b) polarization extinction ration (PER).

Table 1. Circular polarization characteristics for designed CMM at resonances.

Operation frequency (GHz)	PER (dB)	Ellipticity $\eta(^\circ)$	Relative dimension
f_1 (7.15 GHz)	26.1 dB	42.17°	$\lambda_0/11.98 \times \lambda_0/11.98 \times \lambda_0/36.17$
f_2 (9.24 GHz)	−26.2 dB	−42.21°	$\lambda_0/9.27 \times \lambda_0/9.27 \times \lambda_0/36.17$
f_3 (13.22 GHz)	30.1 dB	40.43°	$\lambda_0/6.47 \times \lambda_0/6.47 \times \lambda_0/36.17$
f_4 (15.34 GHz)	23.2 dB	41.29°	$\lambda_0/5.58 \times \lambda_0/5.58 \times \lambda_0/36.17$

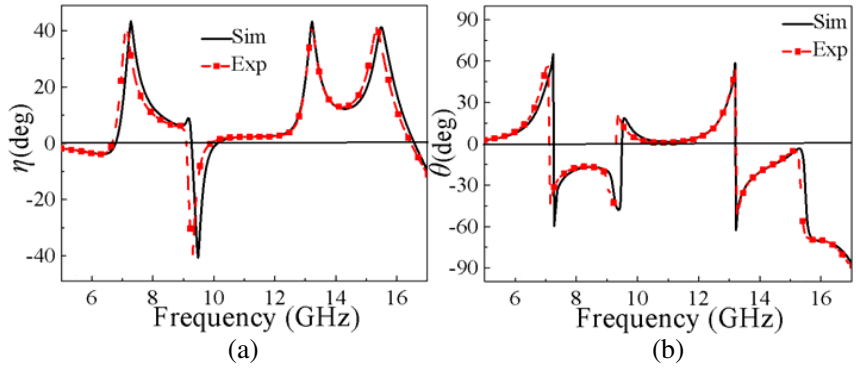

Figure 4. Simulated and measured (a) ellipticity η and (b) polarization azimuth rotation angle θ for the forward $(-z)$ propagation in y polarization.

the designed CMMs slab.

The functionality of multi-band circular polarizer or circular polarization convertor of the proposed CMMs can be further demonstrated through the analysis of ellipticity η and polarization rotation angle θ [22]. According to Eqs. (4) and (5), η and θ for the y-polarized waves propagating along forward $(-z)$ direction can be calculated, respectively. From Fig. 4(a) and Table 1, the experiment (simulation) peak values of η are about 42.17° (43.35°), 40.43° (43.28°), 41.29° (41.02°) and −42.21° (−40.76°) at 7.15 (7.28) GHz, 13.19 (13.22) GHz, 15.34 (15.45) GHz and 9.24 (9.38) GHz, indicating that the transmitted waves are nearly pure circular polarization at the four resonances. Furthermore, from Fig. 4(b), it can be seen that the values of η are zero at 6.65 (6.78) GHz, 9.09 (9.21) GHz, and 16.48 (16.58) GHz, respectively. On the other hand, the values of θ are about 28.47° (28.15°), −29.92° (−40.11°), and −74.65° (−75.22°) when $\eta = 0°$ with respect to the incident linearly polarized wave. Obviously, the transmitted wave is still linear polarization with rotation angle θ at above three frequencies and also indicating giant optical activity. These results further indicate that the designed CMM can function as a nearly perfect circular polarization convertor at resonances. Furthermore, it should be noticed that the size of the unit cell of the designed CMMs is only $\lambda_0/11.98 \times \lambda_0/11.98 \times \lambda_0/36.17$ at 7.15 GHz, where λ_0 is corresponding to the resonance wavelength. Thus, our proposed CMM has some advantages compared with previous CMM in circular polarization extinction ration and ultra-compact structure design [38–40].

Finally, the resonances mechanism of the proposed CMM structure can be understood by examining the surface current distributions. As shown in Fig. 5, surface current distributions in each DSRR layer are investigated at each resonant frequency to analyze the polarization conversion. Intrinsically, the operation mechanism of circular polarizer featured with giant CD effect mainly originates from the interlayer near-field coupling between two twisted layers [31–36]. At resonances, all the field patterns will be twisted inside the slab as a consequence of interlayer longitudinal magnetic dipole to magnetic dipole coupling or transverse electric dipole to electric dipole coupling [11, 14, 18, 36, 42, 43]. Furthermore, the EM fields within metallic layers can be rigorously expressed as series of eigenmodes of the SRRs [41]. From Figs. 5(a1)–(a3), at the first resonance of 7.28 GHz for RCP wave, the surface current directions on both inner and outer rings of three SRR layers are the same, resulting in parallel magnetic dipole moments in outer and inner rings of three layers. From Figs. 5(b1)–(b3) and 5(c1)–(c3), at 13.22 GHz and 15.45 GHz for the RCP wave, the cases become complex. At these two resonances, both the same and opposite direction currents exist on both inner and outer rings of the top and middle SRRs layers, but only the same direction currents exist on both inner and outer rings of the bottom SRRs layer, thus producing the cross-coupling between the electric and magnetic fields in the triple-layer twisted SRRs structure. From Figs. 5(d1)–(d3), at 9.38 GHz for LCP wave, the surface currents on the top and bottom layers are antiparallel for both rings, indicating antiparallel magnetic dipole moments in both layers. The distinguished current direction from the top to bottom layers gives rise to the different rotation directions of the transmitted circularly polarization waves at the four resonant frequencies. These surface current distributions properties effectively explain different transmitted circular polarizations.

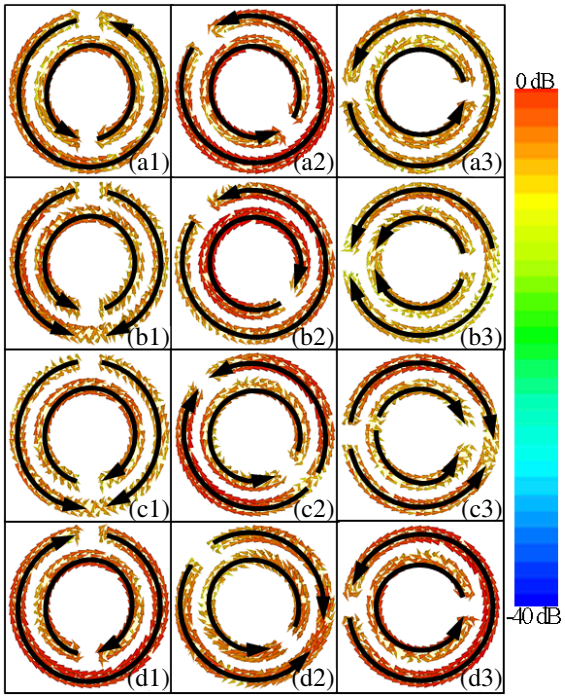

Figure 5. The simulated surface currents distributions for the proposed CMMs in the case of the incident y-polarized wave propagating along $-z$ direction at (a1)–(a3) 7.28 GHz, (b1)–(b3) 13.22 GHz, (c1)–(c3) 15.45 GHz and (d1)–(d3) 9.38 GHz for top layer, middle layer and bottom layer structure. Solid black line arrows denote the current directions.

5. CONCLUSION

In conclusion, an ultra-compact CMMs composed of triple-layers TSRRs structure is proposed and comprehensively characterized by simulation and experiment in microwave region. Simulation results exhibit that it can convert a linearly polarized wave to an RCP waves at 7.28 GHz, 13.22 GHz, and 15.45 GHz and an LCP at 9.38 GHz, respectively, which are in good agreement with the experiments. The unit cell of the designed structure is extremely thin in the longitudinal direction and also very small in the transverse directions compared with the operation wavelength ($\lambda_0/11.98 \times \lambda_0/11.98 \times \lambda_0/36.17$ at 7.15 GHz). Moreover, this ultra-compact structure CMM possesses four resonant bands and high PER of more than 20 dB across four bands. The physical mechanism behind the phenomena has been further illustrated by simulated surface current distributions. This ultra-compact structure CMM with four-band operation can be developed to explore more potential applications where the circular polarizer needs to be integrated with other compact devices, such as electrically small antennas and small sensors.

ACKNOWLEDGMENT

This work is supported by the Joint Funds of the National Natural Science Foundation of China (U1435209).

REFERENCES

1. Pendry, J. B., "A chiral route to negative refraction," *Science*, Vol. 306, No. 19, 1353–1355, 2004.
2. Rogacheva, A. V., V. A. Fedotov, A. S. Schwanecke, and N. I. Zheludev, "Giant gyrotropy due to electromagnetic-field coupling in a bilayered chiral structure," *Phys. Rev. Lett.*, Vol. 97, No. 17, 177401, 2006.

3. Plum, E., J. Zhou, J. Dong, V. A. Fedotov, T. Koschny, C. M. Soukoulis, and N. I. Zheludev, "Metamaterial with negative index due to chirality," *Phys. Rev. B*, Vol. 79, No. 3, 035407(6), 2009.
4. Zhou, J., J. Dong, B. Wang, T. Koschny, M. Kafesaki, and C. M. Soukoulis, "Negative refractive index due to chirality," *Phys. Rev. B*, Vol. 79, No. 12, 121104(3), 2009.
5. Li, Z., R. Zhao, T. Koschny, M. Kafesaki, K. B. Alici, E. Colak, H. Caglayan, E. Ozbay, and C. M. Soukoulis, "Chiral metamaterials with negative refractive index based on four "U" split ring resonators," *Appl. Phys. Lett.*, Vol. 97, No. 8, 081901(2), 2010.
6. Cheng, Y., Y. Nie, and R. Z. Gong, "Giant optical activity and negative refractive index using complementary U-shaped structure assembly," *Progress In Electromagnetics Research M*, Vol. 25, 239–253, 2012.
7. Decker, M., M. W. Klein, M. Wegener, and S. Linden, "Circular dichroism of planar chiral magnetic metamaterials," *Opt. Lett.*, Vol. 32, No. 7, 856–858, 2007.
8. Cheng, Y., Y. Nie, L. Wu, and R. Z. Gong, "Giant circular dichroism and negative refractive index of chiral metamaterial based on split-ring resonators," *Progress In Electromagnetics Research*, Vol. 138, 421–432, 2013.
9. Lee, S., Z. Wang, C. Feng, J. Jiao, A. Khan, and L. Li, "Circular dichroism in planar extrinsic chirality metamaterial at oblique incident beam," *Opt. Commun.*, Vol. 309, 201–204, 2013.
10. Menzel, C., C. Helgert, C. Rockstuhl, E.-B. Kley, A. Täunnermann, T. Pertsch, and F. Lederer, "Asymmetric transmission of linearly polarized light at optical metamaterials," *Phys. Rev. Lett.*, Vol. 104, 253902, 2010.
11. Wei, Z., Y. Cao, Y. Fan, X. Yu, and H. Li, "Broadband polarization transformation via enhanced asymmetric transmission through arrays of twisted complementary split-ring resonators," *Appl. Phys. Lett.*, Vol. 99, No. 22, 221907-3, 2011.
12. Huang, C., Y. Feng, J. Zhao, Z. Wang, and T. Jiang, "Asymmetric electromagnetic wave transmission of linear polarization via polarization conversion through chiral metamaterial structures," *Phys. Rev. B*, Vol. 85, 195131, 2012.
13. Dincer, F., C. Sabah, M. Karaaslan, E. Unal, M. Bakir, and U. Erdiven, "Asymmetric transmission of linearly polarized waves and dynamically wave rotation using chiral metamaterial," *Progress In Electromagnetics Research*, Vol. 140, 227–239, 2013.
14. Cheng, Y. Z., Y. Nie, X. Wang, and R. Z. Gong, "An ultrathin transparent metamaterial polarization transformer based on a twist-split-ring resonator," *Appl. Phys., A Mater. Sci. Process.*, Vol. 111, No. 1, 209–215, 2013.
15. Wu, L., Z. Yang, Y. Cheng, R. Gong, M. Zhao, Y. Zheng, J. Duan, and X. Yuan, "Circular polarization converters based on bi-layered asymmetrical split ring metamaterials," *Applied Physics A*, Vol. 116, No. 2, 643–648, 2014.
16. Ma, X., C. Huang, M. Pu, W. Pan, Y. Wang, and X. Luo, "Circular dichroism and optical rotation in twisted Y-shaped chiral metamaterial," *Appl. Phys. Exp.*, Vol. 6, 022001, 2013.
17. Jackson, J. D., *Classical Electrodynamics*, 3rd Edition, 205–207, Wiley, 1999.
18. Liu, N., H. Liu, S. Zhu, and H. Giessen, "Stereometamaterials," *Nat. Photon.*, Vol. 3, 157–162, 2009.
19. Decker, M., R. Zhao, C. M. Soukoulis, S. Linden, and M. Wegener, "Twisted split-ring-resonator photonic metamaterial with huge optical activity," *Opt. Lett.*, Vol. 35, No. 2, 1593–1595, 2010.
20. Powell, D. A., K. Hannam, I. V. Shadrivov, and Y. S. Kivshar, "Near-field interaction of twisted split-ring resonators," *Phys. Rev. B*, Vol. 83, 235420, 2011.
21. Liu, M., D. A. Powell, I. V. Shadrivov, and Y. S. Kivshar, "Optical activity and coupling in twisted dimer meta-atoms," *Appl. Phys. Lett.*, Vol. 100, 111114, 2012.
22. Li, Z., M. Mutlu, and E. Ozbay, "Chiral metamaterials: From optical activity and negative refractive index to asymmetric transmission," *J. Opt.*, Vol. 15, 023001, 2013.
23. Li, M., L. Guo, and H. Yang, "Experimental and simulated study of dual-band chiral metamaterials with strong optical activity," *Microwave and Optical Technology Letters*, Vol. 56, No. 10, 2381–2385, 2014.

24. Hannam, K., D. A. Powell, I. V. Shadrivov, and Y. S. Kivshar, "Broadband chiral metamaterials with large optical activity," *Phys. Rev. B*, Vol. 89, 125105, 2014.
25. Zhao, Y., A. Belkin, and A. Alù, "Twisted optical metamaterials for planarized ultrathin broadband circular polarizers," *Nat. Commun.*, Vol. 3, 870, 2012.
26. Chen, J. and A. Zhang, "A novel design of circularly polarized antenna based on metamaterial," *International Journal of Electronics*, Vol. 100, No. 6, 770–778, 2013.
27. Hong, Q., T. Wu, X. Zhu, R. Lu, and S. T. Wu, "Designs of wide-view and broadband circular polarizers," *Opt. Express*, Vol. 13, No. 20, 8318–8331, 2005.
28. Ge, Z., M. Jiao, R. Lu, T. X. Wu, S. T. Wu, W. Y. Li, and C. K. Wei, "Wide-view and broadband circular polarizers for transflective liquid crystal displays," *J. Display Technol.*, Vol. 4, No. 2, 129–138, 2008.
29. Gansel, J., M. Thiel, M. S. Rill, M. Decker, K. Bade, V. Saile, G. von Freymann, S. Linden, and M. Wegener, "Gold helix photonic metamaterial as broadband circular polarizer," *Science*, Vol. 325, No. 5947, 1513–1515, 2009.
30. Mutlu, M., A. E. Akosman, A. E. Serebryannikov, and E. Ozbay, "Asymmetric chiral metamaterial circular polarizer based on four U-shaped split ring resonators," *Opt. Lett.*, Vol. 36, No. 9, 1653–1655, 2011.
31. Ma, X., C. Huang, M. Pu, C. Hu, Q. Feng, and X. Luo, "Multi-band circular polarizer using planar spiral metamaterial structure," *Opt. Express*, Vol. 20, No. 14, 16050–16058, 2012.
32. Xie, L., H.-L. Yang, X. Huang, and Z. Li, "Multi-band circular polarizer using archimedean spiral structure chiral metamaterial with zero and negative refractive index," *Progress In Electromagnetics Research*, Vol. 141, 645–657, 2013.
33. Yana, S. and G. A. E. Vandenbosch, "Compact circular polarizer based on chiral twisted double split-ring resonator," *Appl. Phys. Lett.*, Vol. 102, 103503, 2013.
34. Xu, H. X., G. M. Wang, M. Q. Qi, T. Cai, and T. J. Cui, "Compact dual-band circular polarizer using twisted Hilbert-shaped chiral metamaterial," *Opt. Express*, Vol. 210, No. 21, 24912–24921, 2013.
35. Ye, Y., X. Li, F. Zhuang, and S. W. Chang, "Homogeneous circular polarizers using a bilayered chiral metamaterial," *Appl. Phys. Lett.*, Vol. 99, 031111, 2011.
36. Cheng, Y., Y. Nie, Z. Cheng, and R. Z. Gong, "Dual-band circular polarizer and linear polarization transformer based on twisted split-ring structure asymmetric chiral metamaterial," *Progress In Electromagnetics Research*, Vol. 145, 263–272, 2014.
37. Euler, M., V. Fusco, R. Cahill, and R. Dickie, "325 GHz single layer sub-millimeter wave FSS based split slot ring linear to circular polarization convertor," *IEEE Trans. Antenn. Propag.*, Vol. 58, No. 7, 2457–2458, 2010.
38. Wu, S., X. Huang, B. Xiao, Y. Jin, and H. Yang, "Multi-band circular polarizer based on twisted triple split-ring resonator," *Chin. Phys. B*, Vol. 23, No. 12, 127805, 2014.
39. Li, Y., J. Zhang, S. Qu, J. Wang, L. Zheng, Y. Pang, Z. Xu, and A. Zhang, "Achieving wide-band linear-to-circular polarization conversion using ultra-thin bi-layered metasurfaces," *Journal of Applied Physics*, Vol. 117, No. 4, 044501, 2015.
40. Hodgkinson, I. J., A. Lakhtakia, Q. H. Wu, S. L. De, and M. W. McCall, "Ambichiral, equichiral and finely chiral layered structures," *Opt. Commun.*, Vol. 239, 353, 2004.
41. Cheng, Y. Z., Y. Nie, Z. Z. Cheng, L. Wu, X. Wang, and R. Z. Gong, "Broadband transparent metamaterial linear polarization transformer based on triple-split-ring resonators," *Journal of Electromagnetic Waves and Applications*, Vol. 27, No. 14, 1850–1858, 2013.
42. Cheng, Y. Z., R. Z. Gong, Z. Z. Cheng, and Y. Nie, "Perfect dual-band circular polarizer based on twisted split-ring structure asymmetric chiral metamaterial," *Applied Optics*, Vol. 53, No. 25, 5763–5768, 2014.
43. Cheng, Y. Z., R. Z. Gong, and Z. Z. Cheng, "A photoexcited broadband switchable metamaterial absorber with polarization-insensitive and wide-angle absorption for terahertz waves," *Optics Commun.*, Vol. 361, 41–46, 2016.